Mohammedi Mokhtar Mahmoud[1], Bendiabdellah Azzedine[1], Allaoui Tayeb[2] , Cherif Bilal Djamal Edine[1]

Group Diagnostic, Laboratory of Electrical Drives Development (LDEE), University of Sciences & Technology of Oran Mohamed Boudiaf (USTO-MB) (1), University of Ibn Khaldun, Tiaret Algeria(2)

doi:10.15199/48.2020.10.03

Wind energy conversion system control robustness based on current analysis of IGBT open-circuit fault

Abstract. *This paper deals with the study of the performance of a wind energy conversion system (WECS) based on a doubly fed induction generator (DFIG) under the IGBT open-circuit fault of the rotor side converter (RSC) during the application of robust control techniques, such as backstepping control (BSC) and sliding mode control (SMC). The presence of IGBT open-circuit faults in DFIG-WECS can disrupt service continuity resulting in financial loss. To overcome such a problem, robust control techniques are usually used as a solution. These control techniques are well known for their ability to treat non-linear structures as power electronics converters and to maintain the performance and stability of the DFIG-WECS connected to the network by the back-to-back converter in healthy and faulty operations. The aim of using robust non-linear control techniques is to obtain better performance and to extend the DFIG-WECS functionality in degraded mode in the event of a failure, and consequently to increase its reliability, unlike the proportional integral (PI) controller which shows less robustness when DFIG non-linearities are considered. The results obtained from these control techniques illustrate well the merits and the effectiveness of each of them in the case of healthy and faulty operations, in particular for the BSC technique, which shows a better performance compared to the SMC technique, which faces the main problem associated with discontinuous control.*

Streszczenie. Przedstawiono analizę właściwości systemu energii wiatrowej bazującego na igeneratorze DFIG w obwodzie IGBT z zastosowaniem odpornego sterowania typu backstepping BSC I sterowania ślizgowego SMC. Zastosowano nieliniową technikę sterowania. Badania symulacyjne wykazały odporność systemu zarówno w warunkach zdrowych jak i przy pojawieniu się błędów. ***System przetwarzania energii wiatrowej z odpornym sterowaniem bazującym na analizie prądu w układzie IGBT***

Keywords: open-switch fault, robust control techniques, system performance, current analyses.
Słowa kluczowe: energia wiatrowa, generator DGIG, odporne sterowanie

Introduction

Using robust control techniques to keep system operation under IGBT switch faults appearance until the application of a hardware redundancy intervention to avoid the interruption of service is a crucial issue. The reason is that, one should consider several constraints; among them is the fault detection [1], the reduction of the fault detection needed time [2] and to define the assessment of the power electronic system reliability, such as the failure existence (the time between failure (TBF) until the time to repair (TTR) [3]). The fault-reconfiguration is generally founded on hardware redundancy design [4] [5] and most of the detection and tolerant methods are hardware based.

It is therefore very significant for researchers to study and investigate the influence of the fault occurrence in the robust control techniques presence. To carry out this study, the following system is considered: a wind turbine to extract maximum energy [6], which is integrated to a Doubly-Fed Induction Generator (DFIG). DFIG is one of the most used generator in wind energy applications with the largest part of the installed Wind Energy Conversion Systems (WECS) using the variable speed technology [7] and also for the back-to-back converter and its stability on the sub-synchronous and super-synchronous operating modes [8].

The rotor side converter (RSC) control techniques are widely studied by researchers. The conventional control approaches for the DFIG are built on voltage and flux oriented control techniques [9]. When the DFIG nonlinearities are considered, the classical vector control techniques; using the proportional-integral (PI) [10]; show less robustness and low performance. Hence, the nonlinear control approaches such as the back stepping and sliding mode control techniques have been more useful due to their various properties; their fast dynamic response, their capability to deal with unmodeled dynamics and faults disturbance. These properties are appropriate to control both active and reactive powers [11], but both the sliding mode control (SMC) and the back stepping control (BSC) techniques have been used in the WECS power regulation mode respectively only with the objective to develop the performance and the quality of this powers in the healthy case [12] [13].

The present paper proposes the study of a DFIG-WECS system, to investigate its performance under both the healthy and the faulty cases. The existence of the open-circuit-fault in the RSC IGBT switch can disturb the continuity of service of the system. To overcome such a problem, robust control techniques like BSC and SMC are proposed and used in this paper. The performance of these control techniques have the ability to deal with nonlinear structures and variable configurations like power electronic converters and also to maintain the performance and the stability of the DFIG integrated to a wind-energy turbine linked to the network by the back-to-back converter under healthy and rotor side open-switch fault operations.

The robust control techniques are applied until a hardware redundancy implementation and a future maintenance operation are achieved. The paper also introduces a performance comparative study between the proposed control methods and the results obtained illustrate well the merits of each one of them during faulty conditions.

The proposed system investigated in this paper is a wind system based on a DFIG, which is essentially composed of a doubly-fed induction generator, a back-to-back converter linked to the grid by the grid side converter (GSC) and to the rotor by the rotor side converter (RSC) and a wind turbine supported by an MPPT control. Figure 1 represents the PI controls synoptic scheme of the DFIG-WECS.

1. DFIG-WECS description and modelisation

In the following, the model of each sub-system of the DFIG-WECS is to be presented and discussed.

1.1 Model of the turbine

The turbine is a device that converts the kinetic wind power into mechanical power. The wind power is defined as follows:

(1) $$P_v = \frac{\rho.S.v_v^{\,3}}{2}$$

where: ρ –density of the air, S–circular area swept by the blades of the turbine, V_V–wind speed.

The mechanical power developed on the shaft of a wind turbine is expressed by [11] [14]:

$$P_{aer} = C_p.P_v = C_p(\lambda,\beta).\frac{\rho.S.v_v^3}{2} \tag{2}$$

where: $C_p(\lambda,\beta)$ –power coefficient, λ –specified speed given as:

$$\lambda = \frac{R.\Omega_{turbine}}{v_v} \tag{3}$$

where: $\Omega_{turbine}$ –rotational speed of the turbine, R-radius of the turbine

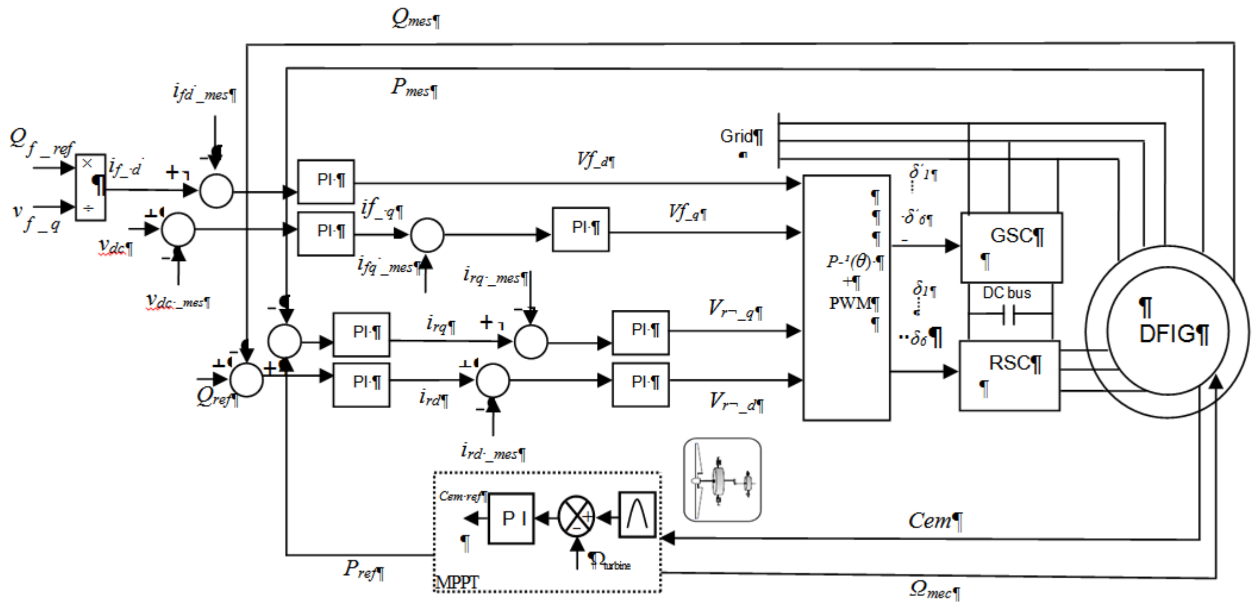

Fig.1. synoptic scheme of the DFIG-WECS based on PI controllers

The expression of the power coefficient is:

$$C_p = 0.5176(\frac{116}{\lambda_i} - 0.4\beta)\exp^{(\frac{21}{\lambda_i})} + 0.0068\lambda_i \tag{4}$$

Where the coefficients of the equation (4) depend on the considered turbine

With:

$$\frac{1}{\lambda_i} = \frac{1}{\lambda + 0.008\beta} - \frac{0.035}{1+\beta^3} \tag{5}$$

The relation between C_p and λ for the given values of the angle of orientation of the blades β is represented by the following figure 2:

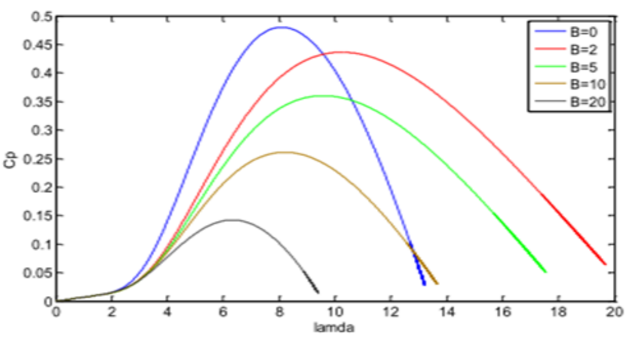

Fig.2. Pitch angle β effect on the aerodynamic coefficient of power

From the power, the wind turbine torque is given by:

$$C_{aer} = \frac{P_{aer}}{\Omega_{turbine}} = C_p.\frac{\rho.S.v^3}{2}.\frac{1}{\Omega_{turbine}} \tag{6}$$

The basic equation of the dynamic allows determining the evolution of the mechanical speed from the overall mechanical torque C_{mec} applied to the rotor:

$$J.\frac{d\Omega_{mec}}{dt} = C_{mec} \tag{7}$$

where: J –overall inertia of the rotor of the generator:

$$J = \frac{J_{turbine}}{G^2} + J_{generator} \tag{8}$$

And G –gain of the speed multiplier.

The mechanical torque takes into account, the electromagnetic torque C_{em} produced by the generator; the torque of the viscous frictions C_{vis} and the torque coming from the multiplier C_g.

$$C_{mec} = C_g - C_{em} - C_{vis} \tag{9}$$

1.2 Speed control and maximum wind power extraction

The control consists to adjust the electromagnetic torque on the DFIG shaft. To accomplish this, one must perform the control of the rotation speed, as shown in Figure 3.

Figure 4 depicts the speed adjustment.

Using the poles compensation method the regulator gains are determined as follow:

$$K_{P\Omega mec} = \frac{J}{\tau} \tag{10}$$

$$K_{i\Omega mec} = \frac{F}{\tau} \tag{11}$$

where

(12) $$\tau = \frac{J}{K_{p\Omega mec}}$$

where F–overall friction coefficient

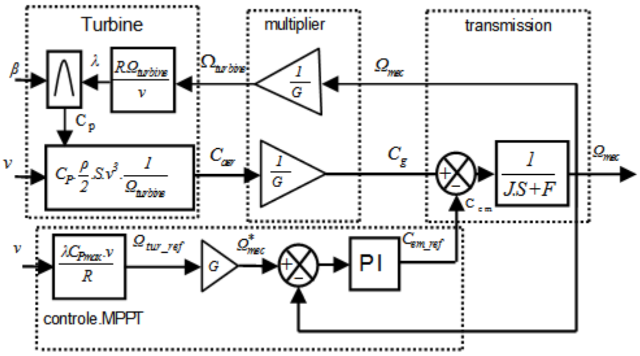

Fig.3. Block diagram of the turbine model With MPPT Control

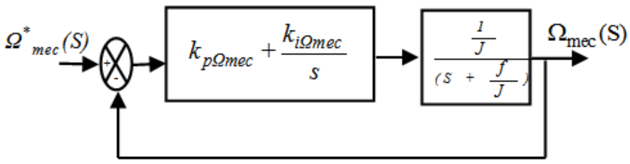

Fig.4. Closed loop for PI speed regulation

1.3 Model of the DFIG

The voltages equations of the DFIG in the d-q reference are [11]:

(13) $$\begin{cases} V_{sd} = R_s i_{sd} + \dfrac{d\Phi_{sd}}{dt} - \omega_s \Phi_{sq} \\ V_{sq} = R_s i_{sq} + \dfrac{d\Phi_{sq}}{dt} + \omega_s \Phi_{sd} \\ V_{rd} = R_r i_{rd} + \dfrac{d\Phi_{rd}}{dt} - \omega_r \Phi_{rq} \\ V_{rq} = R_r i_{rq} + \dfrac{d\Phi_{rq}}{dt} + \omega_r \Phi_{rd} \end{cases}$$

The flux equations in the d-q reference are:

(14) $$\begin{cases} \Phi_{sd} = L_s i_{sd} + M_{sr} i_{rd} \\ \Phi_{sq} = L_s i_{sq} + M_{sr} i_{rq} \\ \Phi_{rd} = L_r i_{rd} + M_{sr} i_{sd} \\ \Phi_{rq} = L_r i_{rq} + M_{sr} i_{sq} \end{cases}$$

The electromagnetic torque of the DFIG is:

(15) $$Cem = p\frac{M_{sr}}{L_s}\left(\Phi_{sq} i_{rd} - \Phi_{sd} i_{rq}\right)$$

The state model presenting the DFIG in the d-q reference associated to the rotating field at the speed of synchronism ω_s is:

(16)
$$\begin{cases} \dot{\Phi}_{sd} = -\dfrac{R_s}{L_s}\Phi_{sd} + \omega_s \Phi_{sq} + \dfrac{R_s M_{sr}}{L_s} i_{rd} + V_{sd} \\ \dot{\Phi}_{sq} = -\omega_s \Phi_{sd} - \dfrac{R_s}{L_s}\Phi_{sq} + \dfrac{R_s M_{sr}}{L_s} i_{rq} + V_{sq} \\ \dot{i}_{rd} = \dfrac{R_s M_{sr}}{\sigma L_r L_s^2}\Phi_{sd} - \dfrac{M_{sr}}{\sigma L_r L_s}\omega \Phi_{sq} - \left[\dfrac{R_r}{\sigma L_r} + \dfrac{R_s M_{sr}^2}{\sigma L_r L_s^2}\right] i_{rd} + \\ +(\omega_s - \omega) i_{rq} - \dfrac{M_{sr}}{\sigma L_r L_s} V_{sd} + \dfrac{1}{\sigma L_r} V_{rd} \\ \dot{i}_{rq} = \dfrac{M_{sr}}{\sigma L_r L_s}\omega \Phi_{sd} + \dfrac{R_s M_{sr}}{\sigma L_r L_s^2}\Phi_{sq} - (\omega_s - \omega) i_{rd} + \\ -\left[\dfrac{R_r}{\sigma L_r} + \dfrac{R_s M_{sr}^2}{\sigma L_r L_s^2}\right] i_{rq} - \dfrac{M_{sr}}{\sigma L_r L_s} V_{sq} + \dfrac{1}{\sigma L_r} V_{rq} \\ \dot{\omega} = \dfrac{P^2 M_{sr}}{L_s J}\left(\Phi_{sq} i_{rd} - \Phi_{sd} i_{rq}\right) - \dfrac{P}{J} Cr - \dfrac{f}{J}\omega \end{cases}$$

where: σ –Blondel dispersion coefficient given as:

(17) $$\sigma = 1 - \left(M_{sr}^2 / L_r . L_s\right)$$

with: R_s and R_r -stator and rotor resistances, L_s and L_r -stator and rotor inductances, M_{sr} -mutual inductance between stator and rotor, ω_s and ω_r -stator and rotor angular speed, Cr –load torque.

1.4 Active and reactive powers vector control

The idea of the stator flux orientation is to align with the d axis of the rotating frame the stator flux hence resulting in Φ_{sq}=0 and $\Phi_{sd}=\Phi_s$. This approach helps the decoupling between the active and the reactive powers.

The equations (13) and (14) become [11] [15] [16]:

(18) $$\begin{cases} \Phi_{sd} = \Phi_s \\ \Phi_{sq} = 0 \end{cases}$$

(19) $$\begin{cases} V_{sd} = 0 \\ V_{sq} = V_s = \omega_s \Phi_s \\ V_{rd} = R_r i_{rd} + \dfrac{d\Phi_{rd}}{dt} - \omega_r \Phi_{rq} \\ V_{rq} = R_r i_{rq} + \dfrac{d\Phi_{rq}}{dt} + \omega_r \Phi_{rd} \end{cases}$$

(20) $$\begin{cases} \Phi_s = L_s i_{sd} + M_{sr} i_{rd} \\ 0 = L_s i_{sq} + M_{sr} i_{rq} \\ \Phi_{rd} = L_r i_{rd} + M_{sr} i_{sd} \\ \Phi_{rq} = L_r i_{rq} + M_{sr} i_{sq} \end{cases}$$

The rotor currents are written in terms of the stator powers as follow:

(21) $$\begin{cases} P_s = -\dfrac{V_s M_{sr}}{L_s} i_{rq} \\ Q_s = -\dfrac{V_s M_{sr}}{L_s} i_{rd} + \dfrac{V_s^2}{L_s \omega_s} \end{cases}$$

(22) $$\begin{cases} i_{rq} = -\dfrac{L_s}{V_s . M_{sr}} . P_s \\ i_{rd} = \dfrac{V_s^2}{\omega_s . L_s} - \dfrac{L_s}{V_s . M_{sr}} . Q_s \end{cases}$$

The voltages control is given by:

(23)
$$\begin{cases} V_{rd} = R_r i_{rd} + \left(L_r - \dfrac{M_{sr}^2}{L_s}\right)\dot{i}_{rd} - g\omega_s\left(L_r - \dfrac{M_{sr}^2}{L_s}\right)i_{rq} \\ V_{rq} = R_r i_{rq} + \left(L_r - \dfrac{M_{sr}^2}{L_s}\right)\dot{i}_{rq} + g\omega_s\left(L_r - \dfrac{M_{sr}^2}{L_s}\right)i_{rd} + \\ +g\dfrac{M_{sr}V_s}{L_s} \end{cases}$$

1.5 RSC and GSC models

The type of used RSC and GSC converters is a two-level three-phase back-to-back converter, both the RSC and the GSC are controlled by the pulse width modulation (PWM) technique. Their mathematical model is represented by the control signals and the output phase voltages [17] as follow:

(24)
$$\begin{bmatrix} v_a \\ v_b \\ v_c \end{bmatrix} = \frac{v_{dc}}{3}\begin{bmatrix} 2 & -1 & -1 \\ -1 & 2 & -1 \\ -1 & -1 & 2 \end{bmatrix}\begin{bmatrix} \delta_1 \\ \delta_2 \\ \delta_3 \end{bmatrix}$$

With: va, vb, vc –output phase voltages, δ_1, δ_2, δ_3 - PWM top switches gates control signals, v_{dc} -DC bus voltage.

1.5.1 Grid side control

The currents grid side control leads to the following equations:

(25)
$$\begin{cases} v_{fd} = R_f . i_{fd} + L_f \dot{i}_{fd} + e_{fd} \\ v_{fq} = R_f . i_{fq} + L_f \dot{i}_{fq} + e_{fq} \end{cases}$$

with

(26)
$$\begin{cases} e_{fd} = \omega_s . L_f . i_{fq} \\ e_{fq} = -\omega_s . L_f . i_{fd} + v_{sq} \end{cases}$$

V_{fdq} and i_{fdq}–grid currents and voltages in the d-q reference, L_f and R_f –inductance and resistance of the filter.

1.5.1.1 DC bus voltage v_{dc} control

The dc bus powers are:

(27)
$$\begin{cases} P_{rectifier} = v_{dc} . i_{rectifier} \\ P_{capacitor} = v_{dc} . i_{capacitor} \\ P_{inverter} = v_{dc} . i_{inverter} \end{cases}$$

The relation between these powers is:

(28)
$$P_{rectifier} = P_{capacitor} + P_{inverter}$$

If the filter resistance R_f is neglected, equations (29) and (30) are respectively obtained as:

(29)
$$\begin{cases} P_f = v_{sq} . i_{fq} \\ Q_f = v_{sq} . i_{fd} \end{cases}$$

(30)
$$P_f = P_{rectifier} = P_{capacitor} + P_{inverter}$$

The power reference for the capacitor is:

(31)
$$P^*_{capacitor} = v_{dc} . i^*_{capacitor}$$

The calculation of the power factor is one of the techniques for measuring the quality of energy, the definition of which is given in equation (32) [18].

(32)
$$\begin{cases} PF = \dfrac{P}{S} \\ S^2 = P^2 + Q^2 \end{cases}$$

where: PF -power factor, P -active power measured value, S -apparent power, Q -reactive power measured value.

1.5.2 Rotor side control with power loop

Figure 5 presents Block diagram of the PI indirect control with power loop and Figure 6 gives the functional closed loop of the currents control.

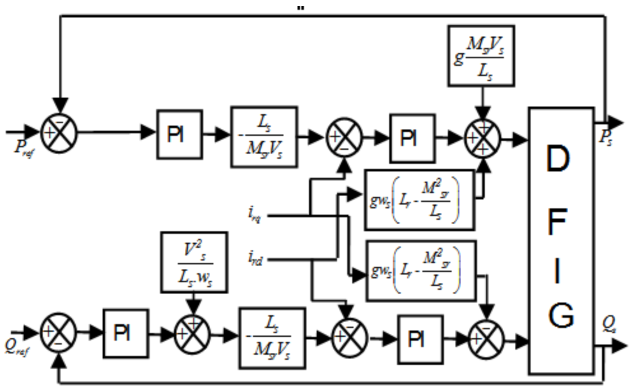

Fig.5. Block diagram of the PI indirect control with power loop

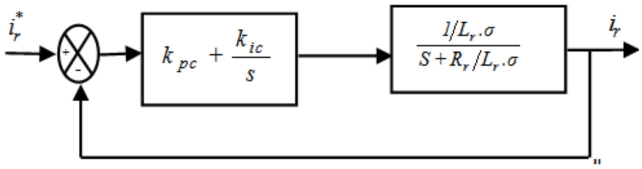

Fig.6. Closed loop for PI currents regulation

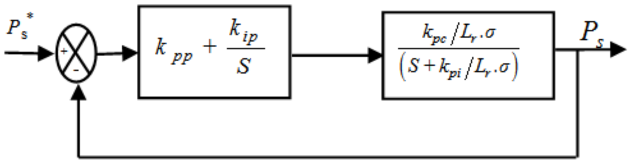

Fig.7. Closed loop for PI powers regulation

By applying the pole compensation method, the regulator gains are determined as:

(33)
$$k_{pc} = \frac{L_r . \sigma}{\tau_1}$$

(34)
$$k_{ic} = \frac{R_r}{\tau_1}$$

with:

(35)
$$\tau_1 = \frac{L_r . \sigma}{k_{pc}}$$

Figure 7 describes the functional closed loop of the powers control.

Again by applying the pole compensation method, the regulator gains are determined as:

(36) $$k_{pp} = \frac{L_r.\sigma}{\tau_2.k_{pc}}$$

(37) $$k_{ip} = \frac{1}{\tau_2}$$

with

(38) $$\tau_2 = \frac{L_r.\sigma}{k_{pp}.k_{pc}}$$

2. Proposed control techniques used

The BSC and the SMC techniques are both robust nonlinear techniques applied to the RSC DFIG-WECS control design with the aim to replace the PI current inner loop controller by the BSC or the SMC.

2.1 BSC applied to the DFIG-WECS

The BSC technique considers the orientation of the stator flux such that $\Phi_{sq}= 0$ and $\Phi_{sd}= \Phi_s$.
The rotor derivatives currents are:

(39) $$\begin{cases} \dot{i}_{rd} = \left(V_{rd} - R_r i_{rd} + g\omega_s L_r \sigma i_{rq}\right)\dfrac{1}{L_r.\sigma} \\ \dot{i}_{rq} = \left(V_{rq} - R_r i_{rq} - g\omega_s L_r \sigma i_{rd} - g\omega_s \dfrac{M_{sr}V_s}{\omega_s L_s}\right) \end{cases}$$

The derivatives of the rotor currents references are given in the equation system (41):

(40) $$\begin{cases} i_{rq}^{ref} = -\dfrac{L_s}{V_s M_{sr}} P_s^{ref} \\ i_{rd}^{ref} = \dfrac{V_s}{\omega_s M_{sr}} - \dfrac{L_s}{V_s M_{sr}} - Q_s^{ref} \end{cases}$$

(41) $$\begin{cases} \dot{i}_{rq}^{ref} = -\dfrac{L_s}{V_s M_{sr}} \dot{P}_s^{ref} \\ \dot{i}_{rd}^{ref} = -\dfrac{L_s}{V_s M_{sr}} \dot{Q}_s^{ref} \end{cases}$$

The combination of vector control with BSC allow replacing PI regulators. The calculating of the BSC voltages is based on Lyapunov functions [11], [12], [19], [20]. This control is based on two steps, which are given as follow:

Step 1:
The Lyapunov function is:

(42) $$v = \frac{1}{2}\left(e_1^2 - e_2^2\right)$$

Where the current errors e_1 and e_2 are given as:

(43) $$\begin{cases} e_1 = \left(i_{rq}^{ref} - i_{rq}\right) \\ e_2 = \left(i_{rd}^{ref} - i_{rd}\right) \end{cases}$$

The derivatives of these errors are:

(44) $$\begin{cases} \dot{e}_1 = \left(\dot{i}_{rq}^{ref} - \dot{i}_{rq}\right) \\ \dot{e}_2 = \left(\dot{i}_{rd}^{ref} - \dot{i}_{rd}\right) \end{cases}$$

The solutions of the null Lyapunov derivative function are:

(45) $$\left(\dot{e}_1 = -K_1.e_1\right) and \left(\dot{e}_2 = -K_2.e_2\right)$$

With: K_1 and K_2 –positive gains.

By replacing (39) and (41) in (44), one obtains:

(46) $$\begin{cases} \dot{e}_1 = \left(\left(-\dfrac{L_s}{M_{sr}V_s}\dot{P}_s^{ref}\right) - \dfrac{1}{L_r\sigma}\begin{pmatrix} V_{rq} - R_r i_{rq} - g\omega_s L_r \sigma i_{rd} + \\ -g\dfrac{M_{sr}V_s}{L_s} \end{pmatrix}\right) \\ \dot{e}_2 = \left(\left(-\dfrac{L_s}{M_{sr}V_s}\dot{Q}_s^{ref}\right) - \dfrac{1}{L_r\sigma}\left(V_{rd} - R_r i_{rd} + g\omega_s L_r \sigma i_{rq}\right)\right) \end{cases}$$

Step 2:
Replacing the derivatives of the error by their values, we obtain:

(47) $$\begin{cases} -K_1 e_1 = \left(\left(-\dfrac{L_s}{M_{sr}V_s}\dot{P}_s^{ref}\right) - \dfrac{1}{L_r\sigma}V_{rq} - \dfrac{1}{L_r\sigma}\begin{pmatrix} -R_r i_{rq} - g\omega_s L_r \sigma i_{rd} + \\ -g\dfrac{M_{sr}V_s}{L_s} \end{pmatrix}\right) \\ -K_2 e_2 = \left(\left(-\dfrac{L_s}{M_{sr}V_s}\dot{Q}_s^{ref}\right) - \dfrac{1}{L_r\sigma}V_{rd} - \dfrac{1}{L_r\sigma}\left(-R_r i_{rd} + g\omega_s L_r \sigma i_{rq}\right)\right) \end{cases}$$

The BSC voltage law is:

(48) $$\begin{cases} V_{rq} = \begin{pmatrix} L_r\sigma\left(-\dfrac{L_s}{M_{sr}V_s}\dot{P}_s^{ref} + K_1 e_1\right) + R_r i_{rq} + g\omega_s L_r \sigma i_{rd} + \\ +g\dfrac{M_{sr}V_s}{L_s} \end{pmatrix} \\ V_{rd} = \left(L_r\sigma\left(-\dfrac{L_s}{M_{sr}V_s}\dot{Q}_s^{ref} + K_2 e_2\right) + R_r i_{rd} - g\omega_s L_r \sigma i_{rq}\right) \end{cases}$$

The diagram represented by Figure 8 depicts the application of the hybrid BSC to the DFIG.

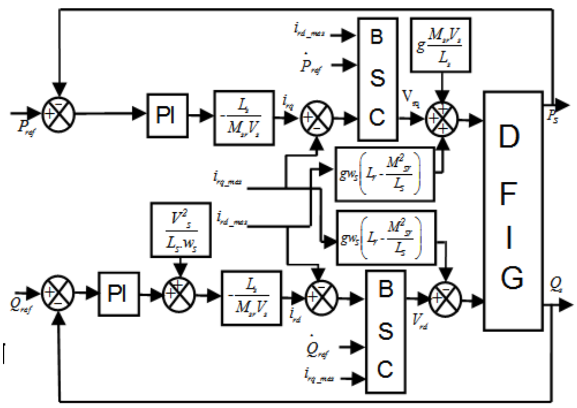

Fig.8. Block diagram of the hybrid BSC

2.2 SMC applied to the DFIG-WECS

The SMC is another powerful nonlinear controller, which attracts many researchers and has been successfully applied in the DFIG-WECS [13], [21], with the idea to attract the states of the DFIG-WECS in a suitable selected area then design a control law that maintain the system in this area [22].

A) Selection of the sliding surfaces s(P_s) and s(Q_s)
The rotor currents i_{rq} and i_{rd} are respectively images of the active and reactive powers. For that, the powers control areas expression is:

(49) $$\begin{cases} s(P_s)=\left(i_{rq}^{ref}-i_{rq}\right) \\ s(Q_s)=\left(i_{rd}^{ref}-i_{rd}\right) \end{cases}$$

B) Convergence condition

The efficiency of the SMC is conditioned by verifying the following Lyapunov relationship of attraction:

$s(x).\dot{s}(x)\le 0$.

C) SMC law calculation

The control algorithm is identified by:

(50) $$u=u^{eq}+u^{attr}$$

$$u^{attr}=u^{max}.sign\left(s(x)\right)$$

Where: u–control variable, u^{eq}–equivalent command, u^{attr}–term control switch and $sign(s(x))$ –sign function.

Let us now apply the SMC to the RSC DFIG-WECS.

1. The reactive power control area and its d axis derivative expressions are given by:

(51) $$s(Q_s)=\left(i_{rd}^{ref}-i_{rd}\right)$$

(52) $$\dot{s}(Q_s)=\left(\dot{i}_{rd}^{ref}-\dot{i}_{rd}\right)$$

When replacing the currents $\dot{i}_{rd}$ and $\dot{i}_{rd}^{ref}$ by their expressions, it is found:

(53) $$\dot{s}(Q_s)=\left(\frac{V_s}{\omega_s.M_{sr}}-\frac{L_s}{V_s.M_{sr}}.\dot{Q}_s^{ref}\right)-\frac{1}{L_r.\sigma}\left(\begin{matrix}V_{rd}-R_r.i_{rd}+\\+g.\omega_s.L_r.\sigma.i_{rq}\end{matrix}\right)$$

(54) $$\begin{cases}\dot{s}(Q_s)=\left(\frac{V_s}{\omega_s.M_{sr}}-\frac{L_s}{V_s.M_{sr}}.\dot{Q}_s^{ref}\right)+\\ -\frac{1}{L_r.\sigma}.V_{rd}-\frac{1}{L_r.\sigma}\left(-R_r.i_{rd}+g.\omega_s.L_r.\sigma.i_{rq}\right)\end{cases}$$

(55) $$\begin{cases}V_{rd}=L_r.\sigma\left(\frac{V_s}{\omega_s.M_{sr}}-\frac{L_s}{V_s.M_{sr}}.\dot{Q}_s^{ref}\right)+R_r.i_{rd}+\\ -g.\omega_s.L_r.\sigma.i_{rq}+L_r.\sigma.v_2.sgn\left(s(Q)\right)\end{cases}$$

The control voltage is defined by the relation: $V_{rd}=V_{rd}^{eq}+V_{rd}^{attr}$

Through the sliding mode at steady state, $s(Q_s)=0$, $d(s(Q_s))=0$, $V_{rd}^{attr}=0$, so the equivalent control is given by:

(56) $$V_{rd}^{eq}=L_r.\sigma\left(\frac{V_s}{\omega_s.M_{sr}}-\frac{L_s}{V_s.M_{sr}}.\dot{Q}_s^{ref}\right)+R_r.i_{rd}-g.\omega_s.L_r.\sigma.i_{rq}$$

Through the convergence mode, the condition $s(x).\dot{s}(x)\le 0$ should be verified with the relation (57):

(57) $$V_{rd}^{attr}=L_r.\sigma.v_2.sgn\left(s(Q_s)\right)$$

Where the product term $(L_r.\sigma.v_2)$ is a positive gain.

2. Similarly, the active power control area and its q axis derivative expressions are given by:

(58) $$s(P_s)=\left(i_{rq}^{ref}-i_{rq}\right)$$

(59) $$\dot{s}(P_s)=\left(\dot{i}_{rq}^{ref}-\dot{i}_{rq}\right)$$

When replacing the currents $\dot{i}_{rq}$ and $\dot{i}_{rq}^{ref}$ by their expressions, we find:

(60) $$\dot{s}(P_s)=-\frac{L_s}{V_s.M_{sr}}.\dot{P}_s^{ref}-\frac{1}{L_r.\sigma}\left(\begin{matrix}V_{rq}-R_r.i_{rq}-g.\omega_s.L_r.\sigma.i_{rd}+\\-g\frac{V_sM_{sr}}{L_s}\end{matrix}\right)$$

(61) $$\begin{cases}\dot{s}(P_s)=-\frac{L_s}{V_s.M_{sr}}.\dot{P}_s^{ref}-\frac{1}{L_r.\sigma}.V_{rq}+\\ -\frac{1}{L_r.\sigma}\left(-R_r.i_{rq}-g.\omega_s.L_r.\sigma.i_{rd}-g\frac{V_sM_{sr}}{L_s}\right)\end{cases}$$

(62) $$\begin{cases}V_{rq}=-\frac{L_s.L_r.\sigma}{V_s.M_{sr}}.\dot{P}_s^{ref}+R_r.i_{rq}+g.\omega_s.L_r.\sigma.i_{rd}+\\ +g.\frac{V_s.M_{sr}}{L_s}+L_r.\sigma.v_1.sgn\left(s(P)\right)\end{cases}$$

The control voltage is defined by: $V_{rq}=V_{rq}^{eq}+V_{rq}^{attr}$

Through the sliding mode and in the steady state, $s(P_s)=0$, $d(s(P_s))=0$, $V_{rq}^{attr}=0$ so the equivalent control is given by:

(63) $$V_{rq}^{eq}=-\frac{L_s.L_r.\sigma}{V_s.M_{sr}}.\dot{P}_s^{ref}+R_r.i_{rq}+g.\omega_s.L_r.\sigma.i_{rd}+g\frac{V_s.M_{sr}}{L_s}$$

Through the convergence mode, the condition $s(x).\dot{s}(x)\le 0$ should be verified with the relation (64):

(64) $$V_{rq}^{attr}=L_r.\sigma.v_1.sgn\left(s(P_s)\right)$$

Where the product term: $(L_r.\sigma.v_1)$–a positive gain.

The diagram shown in Figure 9 represents the application of the hybrid SMC to the DFIG

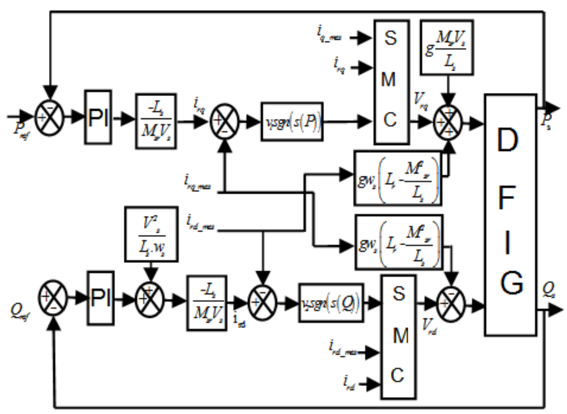

Fig.9. Block diagram of the hybrid SMC

3. Simulation results

The proposed control techniques are supported by a simulation study using the Matlab / Simulink environment to verify their effectiveness. The simulation results are conducted to investigate the performance of a wind turbine related to a 7.5 MW DFIG, a three-phase voltage source at the stator with a sinusoidal network of 220/380V, 50 HZ and with the RSC and GSC switches commutation frequency fixed at 2KHZ. All simulation results related to control techniques are studied and presented for healthy and faulty operations.

3.1 DFIG-WECS in the healthy case

A) Use of the classical PI controllers

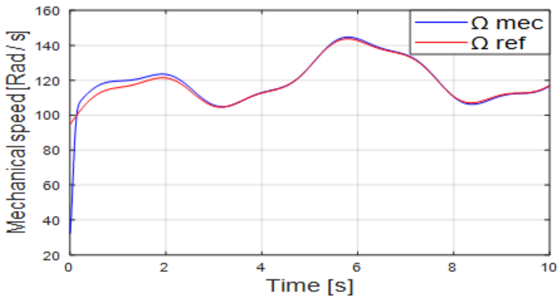

Fig.10. Mechanical speed

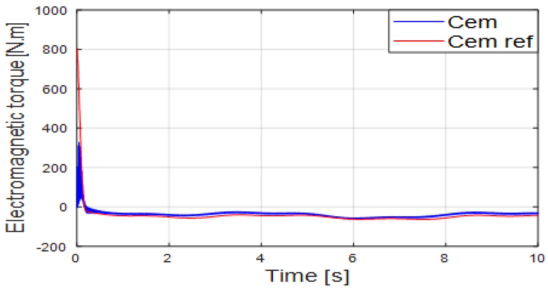

Fig.11. Electromagnetic torque

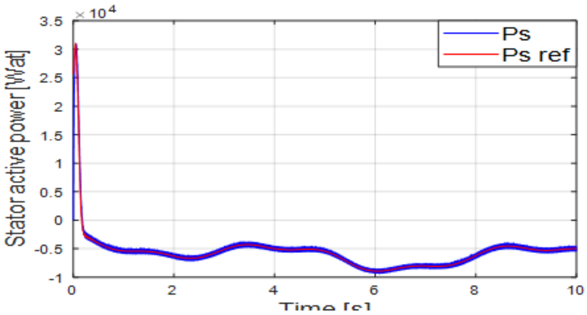

Fig.12. Stator active power

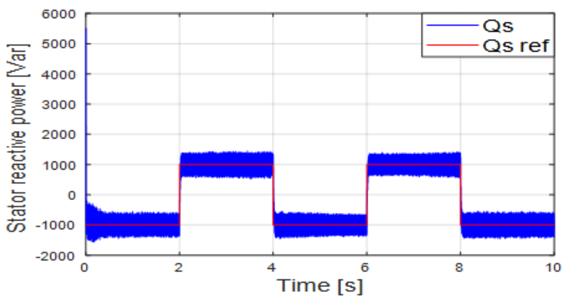

Fig.13. Stator reactive power

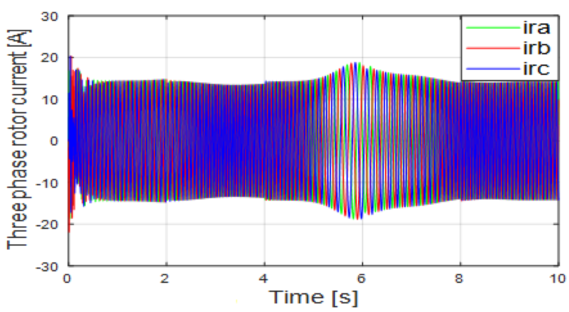

Fig.14. Three-phase rotor current

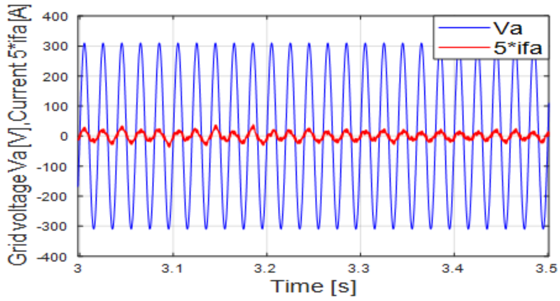

Fig.15. Current *ifa* and grid voltage *Va*

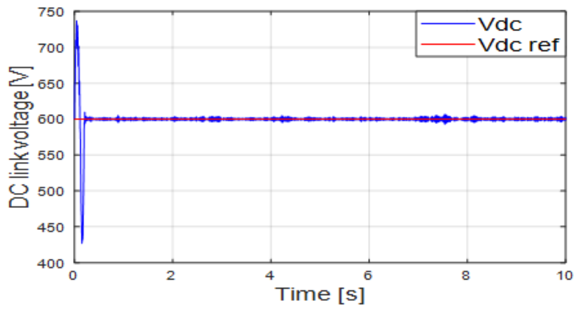

Fig.16.DC link voltage

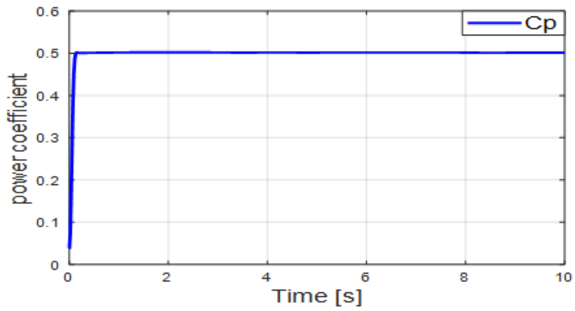

Fig.17. Power coefficient *Cp*

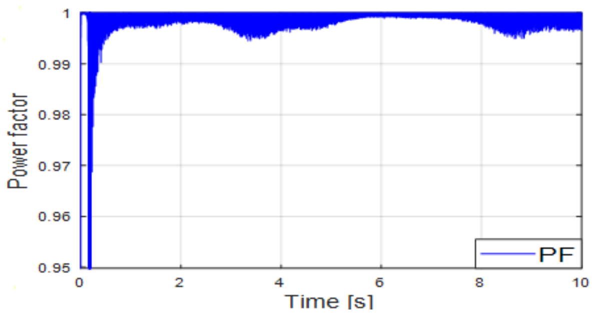

Fig.18. Power factor

The model of the applied wind profile reference [23] is expressed by a summation of several harmonics in a deterministic form given by:

$$v_v(t) = 6.5 + (0.5 * \sin(0.1047 * t) + 2 * \sin(0.2665 * t) + \sin(1.2930 * t) + 0.2 * \sin(3.6645 * t)) \tag{65}$$

To extract the maximum of the wind active power, the angle
of orientation of the blades is chosen to be β=0.

The DFIG rotor mechanical speed is determined by the available speed at the turbine stage shown in figure 03. Figure 10 shows a good following of the mechanical speed *Ω mec* to it reference *Ω ref* in the presence of the PI-MPPT controller. From this control study, it results an electromagnetic torque reference *Cem ref*. The staror active power reference is obtained from:

(66) $$Ps\ ref = Cem\ ref \times \Omega\ mec$$

Figures 12 and 13 depict a good tracking of the active power *Ps* to it reference *Ps ref* and the reactive power *Qs* to it reference *Qs ref* in the presence of the PI powers controllers. As a result and in a closed loop system, the electromagnetic torque *Cem* shown in Figure 11 follows well its reference *Cem ref*.

Figure 14 depicts the sinusoidal form of the three-phase rotor currents (*ira, irb, irc*) in the (a, b, c) referential included between [-15, 15 A]. Whereas, the rotor current increase between the interval [5, 6 s] is due to the optimal stator active power reference determined by the available power at the turbine stage shown by equation (66). This affects the currents in relation to the mechanical speed increase between [5, 6 s] shown in figure 10. This study is carried out with the aim of reaching a point of maximum MPPT tracking power. It is to be noted that in Figure 15, the grid phase voltage *Va* and its current *ifa* are shown when the DFIG operates at sub-synchronous mode. Figure 16 represents the control of the DC bus voltage *vdc* which depicts a good tracking of the reference *vdc ref* = 600v in the presence of the PI controller. Figure 17 represents the power coefficient *Cp*. Finally, Figure 18 represents the power factor *PF* performance when the stator reactive power is fixed at Qs *ref* =0 Var, which is for a near unity power factor case. This is a significant indication for the good effect of the controller for the grid power factor.

B) Use of the robust BSC and SMC techniques in the RSC:

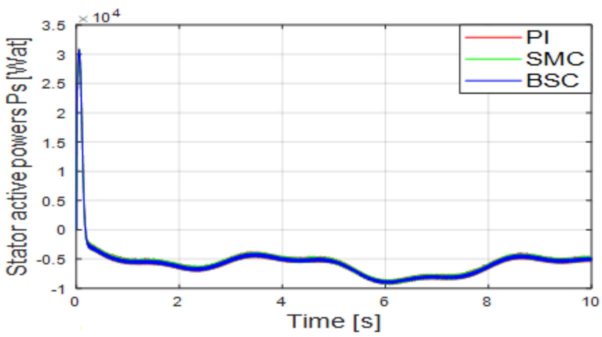

Fig.19. Measured stator active powers

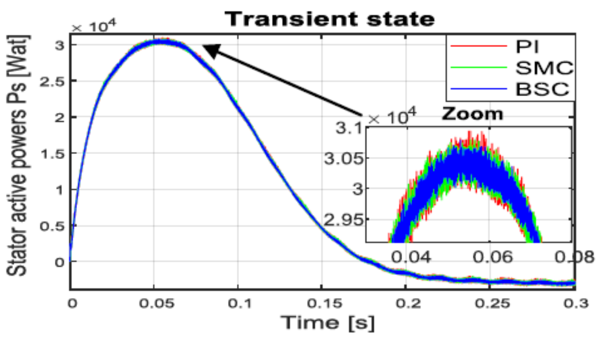

Fig.20. Measured stator active powers under transient state

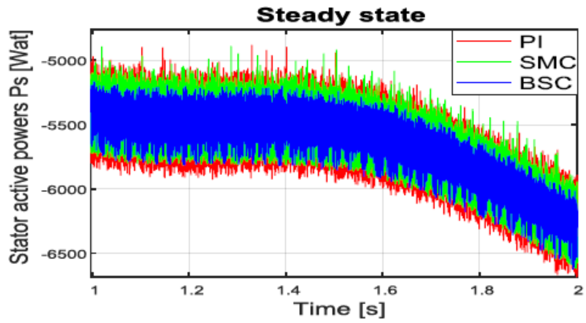

Fig.21. Measured stator active powers under steady state

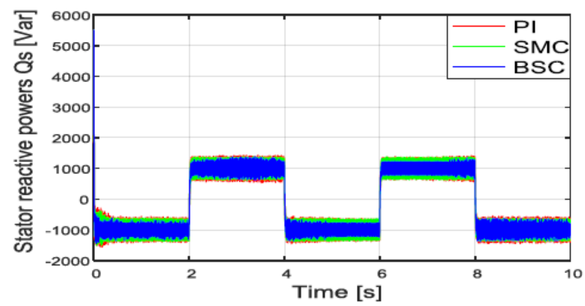

Fig.22. Measured stator reactive powers

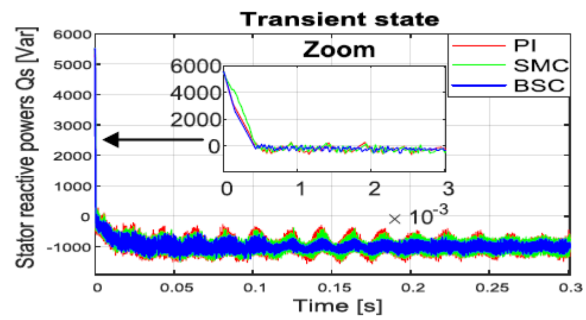

Fig.23. Measured stator reactive powers under transient state

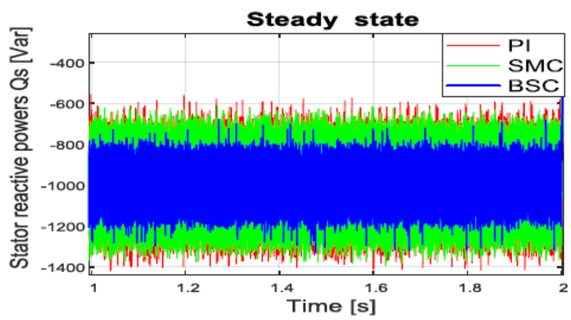

Fig.24. Measured stator reactive powers under steady state

The simulation results obtained when applying robust control techniques as highlighted by the various figures above, show a good performance and an increasing improvement with respect to the classical PI controllers. This is obviously observed from the overshoots and the thickness of the measured values in both transient and steady state conditions. The transient sates of the active and reactive powers as shown respectively by figures 20, 23, illustrate well the enhanced convergence to the steady state of the proposed control techniques compared to the PI controller. On the other hand, the steady states of the active and reactive powers as depicted respectively by figures 21, 24, show the controls overshoots of the active powers measured values. These are respectively represented by the following intervals at time t = 1s: [-5900, -5000 Wat] for the PI controller, [-5700, -5100 Wat] for the SMC technique, [-5600, -5200 Wat] for the BSC technique. The controls overshoots of the reactive powers measured values shown by figure 24 are respectively represented by the following intervals [-1400, -550 Var] for the PI controller, [-1350, -650 Var] for the SMC technique and, [-1280, -700 Var] for the BSC technique. It can be therefore concluded that the BSC technique gives a minimized overshoots response compared to the PI controller and the SMC technique. This does not prevent that one of the strong points of the robust control techniques lies in the good decoupling between the two components of the stator-generated powers. The proposed control techniques using either the BSC or the SMC allows convergence improvement to the steady state with a close to zero steady state error.

3.2 DFIG-WECS current analysis in the faulty case

The aim of using the robust control techniques is to enhance the performance of the DFIG-WECS in the degraded mode, which is defined from the fault appearance until the hardware compensation implementation. The IGBT open-circuit fault is therefore applied twice, in the RSC S_1 switch shown in figure 25, where the faulty leg correspond directly to the current ira. The fault is applied at the beginning of the current ira periods (see section A and B) with the corresponding times, first=1.02s then t=1.06s.

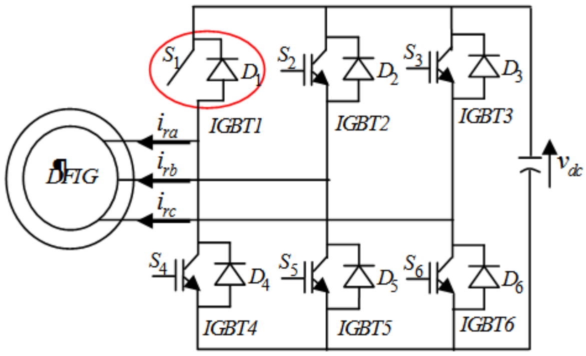

Fig.25. RSC during S_1 switch open-circuit fault

A) Applied fault at time t = 1.02 s with a zoom of one period:

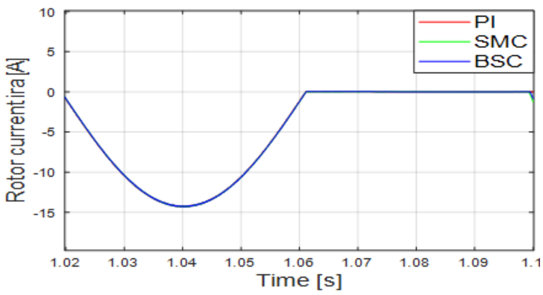

Fig.26. Rotor current ira under fault

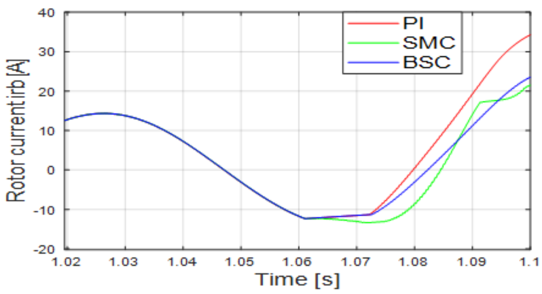

Fig.27. Rotor current irb under fault

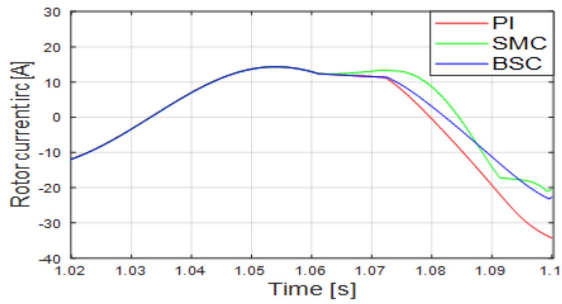

Fig.28. Rotor current irc under fault

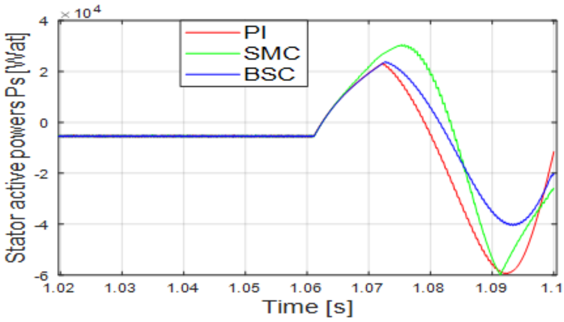

Fig.29. Measured stator active powers under fault

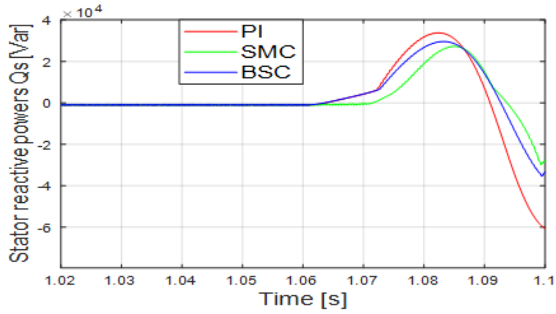

Fig.30. Measured stator reactive powers under fault

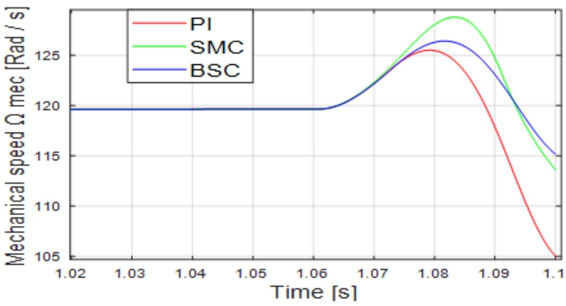

Fig.31. DFIG rotor mechanical speed under fault

B) Applied fault at time t = 1.06 s with a zoom of one period:

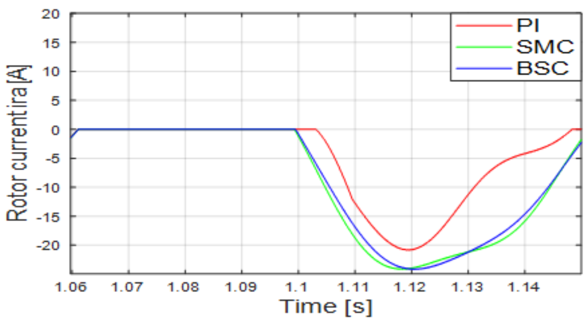

Fig.32. Rotor current ira under fault

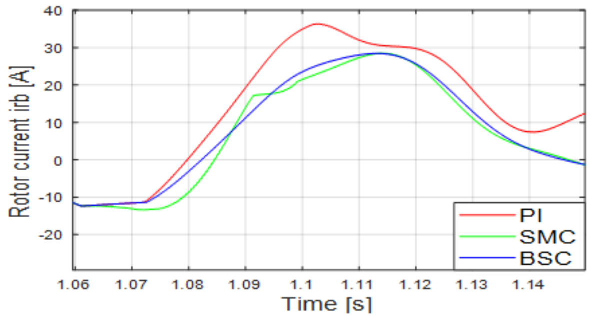

Fig.33. Rotor current irb under fault

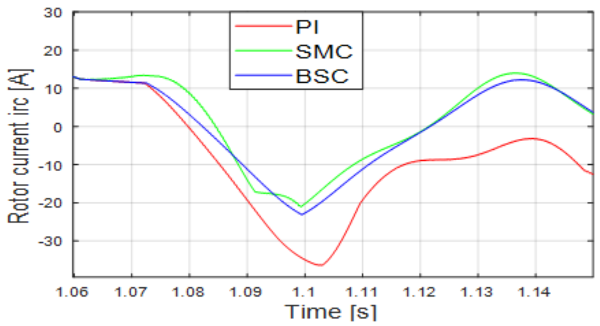

Fig.34. Rotor current irc under fault

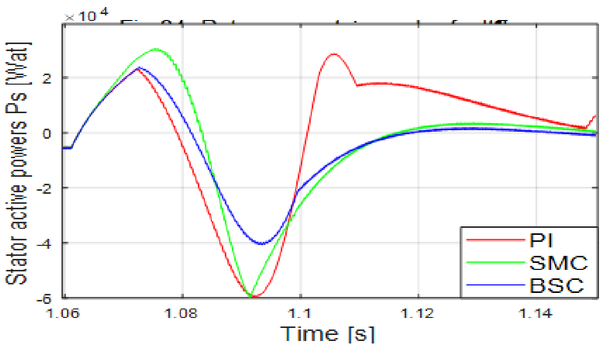

Fig.35. Measured stator active powers under fault

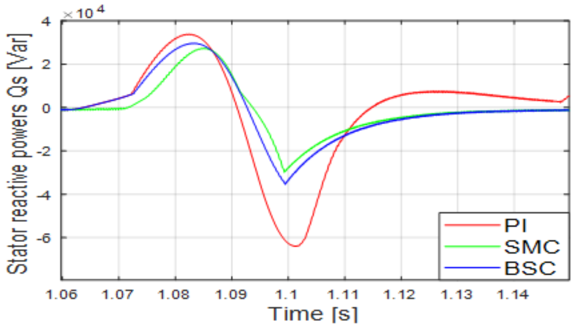

Fig.36. Measured stator reactive powers under fault

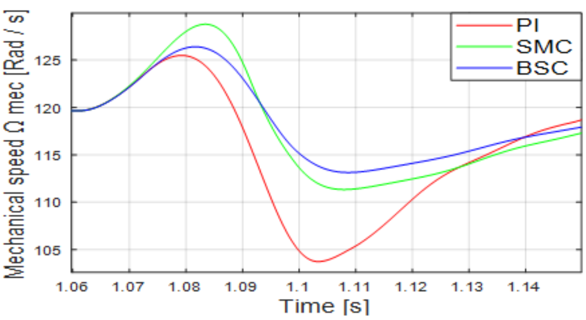

Fig.37. DFIG rotor mechanical speed under fault

Figures 26, 27, 28, 29, 30 and 31 show the behavior of the currents ira , irb and irc, the active and reactive powers and the DFIG rotor mechanical speed measured values when applying an open-circuit fault in the switch S_1 at t=1.02s which corresponds to a beginning of a negative alternation (ira<0 until t=1.06s). During this time interval, in the presence of the open-circuit fault, the diode D_1 allows the current ira to flow in it. It can be seen that the waveforms are not affected and the DFIG-WECS system continues to generate the electrical power in nominal conditions. Now, from t=1.06s until t =1.1s, a positive current ira waveform occurs in the healthy case. It should be noted that in the presence of the inverter IGBT open-circuit fault case and during the blocking period of the diode D1, the current will become zero. The different figures illustrate the behavior of the applied control techniques where it can clearly be seen that the SMC and BSC performances are better than those of the PI controller.

When using SMC or BSC control techniques preceded by fault detection and isolation, the behavior allows the selected applied redundancy to reduce the performance of the DFIG-WECS system to nominal conditions such as that of a healthier condition. When applying the fault at t=1.06s which corresponds to a positive alternation of ira, the same analyses are considered in figures 32, 33, 34, 35, 36 and 37. It should be noted from the figures that the differences in this case is that the diode D1 is immediately blocked after the appearance of the fault and the waveforms are now affected. It is clearly observed from the applied control techniques that the SMC and the BSC show a better performance than the PI controller does even when the negative waveform appear at t=1.1s where it is supposed that the diode D_1 is not blocked and the DFIG-WECS work in nominal conditions. It can be seen from the powers and the DFIG rotor mechanical speed represented respectively by figures 35, 36 and 37, that the DFIG-WECS based on the PI controllers show an important overshoots and a slow restoration into its initials values. On the other hand by using either the BSC or the SMC techniques, we get to minimize the open-circuit fault transient state in fault appearance degraded mode by the enhancement of the fault overshoots and the settling times resulting therefore in a fast dynamic response. This behavior enables the selected applied redundancy to return the DFIG-WECS system performance to the nominal conditions as that of a healthier state case. This confirms the robustness of our proposed control techniques compared to the PI controller. It is also important to know that it is crucial for the continuity of service of the DFIG-WECS to reconfigure the fault immediately after its occurrence by installing a hardware redundancy.

Conclusion

The present paper proposes the study of the performance of a DFIG-WECS under healthy and faulty conditions, where the fault is introduced as an open-circuit fault in the RSC IGBT switches. A performance comparison is carried out to analyze the behavior of the DFIG-WECS under healthy and faulty cases by proposing the use of three RSC control strategies. First a classical indirect PI controller based on the pole compensation is presented and considered as a reference well known approach, then both a hybrid BSC technique based on the stability theory of Lyapunov and a hybrid SMC technique are used. In the healthy case, the BSC and SMC techniques show a good power decoupling performance compared to the PI controller. For the faulty case, the performances of the three control techniques are proposed to investigate how to deal with the RSC open-circuit fault presence. It is found that both the SMC and the BSC techniques show a better performance compared to the PI controller; this is due to the strong power decoupling and the fast response of these robust control techniques. It is important to note that the SMC technique faces the main problem associated with the discontinuous control, which inevitably leads to a chattering phenomenon. This behavior gives a robustness advance margin advantage to the BSC technique compared to the SMC technique. The major objective of the use of the robust control techniques is to benefit from the performance and robustness of the DFGI-WECS and to maintain its operation in acceptable conditions after the fault occurrence until the implementation of a hardware redundancy guaranteeing the continuity of the service.

Authors: *PHD student Mohammedi. Mokhtar. Mahmoud, University of Sciences & Technology Mohamed Boudiaf (USTO-MB), BP 1505 El-M'naouar, Oran, Algeria,*
Email mokhtar.mohammedi@yahoo.fr
Pr. Bendiabdellah. Azeddine, University of Sciences & Technology Mohamed Boudiaf (USTO-MB), BP 1505 El-M'naouar, Oran, Algeria,
Email bendiazz@yahoo.fr
Pr Allaoui. Tayeb, University of Ibn Khaldun, *BP P 78 zaâroura 14000*, Tiaret, Algeria*,*
Email allaoui_tb@yahoo.fr
Dr Cherif. Bilal. Djamal Edine, University of Sciences & Technology Mohamed Boudiaf (USTO-MB), BP 1505 El-M'naouar, Oran, Algeria,
Email cherif.doc84@gmail.com

REFERENCES

[1] Marcelo N., Yves M., Michel K., Jan H., Johan G. (2018) "Robust Power-Electronic Converter Fault Detection and Isolation Technique for DFIG Wind Turbines", IOP Conf. Series: Journal of Physics: Conf. Series 1037 032043 2018.
[2] ZHANG J., CHEN Y., CHEN Z., ZHOU A. (2019) "Open-Switch Fault Diagnosis Method in Voltage-Source Inverters Based on Phase Currents", IEEE access VOLUME 7 doi:10.1109/ACCESS.2019.2913164 .
[3] Stefan B., Elena K., Jyotirmoy R., Ralph G. (2018) "Impact of Component Reliability on Large Scale Photovoltaic Systems' Performance", Energies 2018, 11, 1579; doi:10.3390/en11061579 .
[4] Niraj K., Tapan P., Jitendra K., Krishna K. (2019) "Open‑circuit fault‑tolerance in multilevel inverters with reduced component count" Electrical Engineering, https://doi.org/10.1007/s00202-019-00884-9 2019.
[5] Ajaykumar T., Nita R. (2019) "Fault-tolerant switched capacitor–based boost multilevel inverter" Electrical Engineering, Int J Circ Theor Appl. 2019;1–15., DOI: 10.1002/cta.2671 2019.
[6] Ayushi S., Akhilesh K., Paulson S, (2017) "A Review of MPPT Algorithms Employed in Wind Energy Conversion Systems", Journal of Green Engineering, Vol. 6 4, 385–402, doi: 10.13052/jge1904-4720.643.
[7] Amina Tamer., Djilali Toumi., Azzedine Bendiabdellah., Bilal Djamal Eddine Cherif.,(2017) ''Open Switch Fault Detection and Fault Tolerant of Power Converter Fed DFIG in WECS'', International Review of Automatic Control (I.RE.A.CO.), Vol. 10, N. 3, 2017 Copyright © 2017 Praise Worthy Prize.
[8] Mahalakshmi R., Sindhu T., (2019) "Detailed modelling and development of a laboratory prototype for the analysis of subsynchronous resonance in DFIG□based wind farm", Int Trans Electr Energ Syst.2020;e12245, DOI: 10.1002/2050 7038.12245.
[9] Asha Ram K, (2018) "Vector Control Strategy to Control Active and Reactive Power of Doubly Fed Induction Generator Based Wind Energy Conversion system", Proceedings of the 2nd International Conference on Trends in Electronics and Informatics (ICOEI 2018).
[10] Van T., Nguyen T., Lee D (2015). "Advanced Pitch Angle Control Based on Fuzzy Logic for Variable-Speed Wind Turbine Systems". IEEE Trans. Energy Convers. 2015, PP, 1–10.
[11] Belkacem B., Tayeb A., Mohamed T., Mouloud D, (2019) "Comparative study of back-stepping controller and super twisting sliding mode controller for indirect power control of wind generator", Int J Syst Assur Eng Manag https://doi.org/10.1007/s13198-019-00905-7.
[12] Riyadh Rouabhi ., Chouder Aissa and Ali Djerioui. (2015) "hybride backstepping control of a doubly fed wind energy induction generator "reasearchgate, The Mediterranean Journal of Measurement and Control, Vol. 11 No. 1, 2015.
[13] Riyadh Rouabhi ., Rachid Abdessemed., Aissa Chouder and Ali Djerioui (2015) "Power Quality Enhancement of Grid Connected Doubly-Fed Induction Generator Using Sliding Mode Control" International Review of Electrical Engineering (I.R.E.E.), Vol. 10, N. 2 apr 2015.
[14] OM PRAKASH M., NEERAJ G., MAHDI K., NILESH P, (2019) "Comprehensive Overview of Low Voltage Ride Through Methods of Grid Integrated Wind Generator ", Comprehensive Overview of LVRT Methods of Grid Integrated Wind Generator, VOLUME 7, 2019, DOI 10.1109/ACCESS.2019.2930413.
[15] Nur S., Paul M., Judith M., Yingzhao W, (2018) "DFIG Stator Flux Oriented Control Scheme Execution for Test Facilities Utilising Commercial Converters ", IET Renewable Power Generation 2018, DOI: 10.1049/iet-rpg.2018.5195.
[16] Bossoufi B., Karim M., Lagrioui A., Taoussi M., Derouich A., (2015) "Observer Backstepping control of DFIG-Generators for Wind Turbines Variable-Speed: FPGA Based Implementation" Renewable Energy Journal (ELSIVER), pp 903-917, Vol. 81. September 2015.
[17] Benbouhenni H., Boudjema Z., Belaidi A., Yingzhao W, (2018) "Direct Vector Control of a DFIG Supplied by an Intelligent SVM Inverter for Wind Turbine System ",Iranian Journal of Electrical and Electronic Engineering, Vol. 15, No. 1, March 2019 DOI:10.22068/IJEEE.15.1.45.
[18] Ciprian M., Adriana F., Constantin D., (2020) "Improving the E_ciency and Sustainability of Power Systems Using Distributed Power Factor Correction Methods". Sustainability 2020, 12, 3134; doi:10.3390/su12083134.
[19] Sara M., Ahmed E., Issam M., Tamou N, (2018) "Backstepping Controller for a Variable Wind Speed Energy Conversion System Based on a DFIG ",International Science Index, Electrical and Computer Engineering Vol:12, No:9, 2018 waset.org/Publication/10009495.
[20] Mohamed N., Ahmed E., Tamou N, (2020) "Coordinated Control Using Backstepping of DFIG-Based Wind Turbine for Frequency Regulation in High Wind Energy Penetrated System ",Mathematical Problems in Engineering, Volume 2020, Article ID 8287949, 16 pages, https://doi.org/10.1155/2020/8287949.
[21] Douadi T., Harbouche Y., Abdessemed R.., Bakhti I, (2018) "Improvement Performances of Active and Reactive Power Control Applied to DFIG for Variable Speed Wind Turbine Using Sliding Mode Control and FOC ", International Journal of Engineering (IJE), IJE TRANSACTIONS A: Basics Vol. 31, No. 10, (October 2018) 1689-1697.
[22] Larbi D., Edgar N., Mohammed B, (2020) "First and High Order Sliding Mode Control of a DFIG-Based Wind Turbine ",Electric Power Components and Systems, DOI: 10.1080/15325008.2020.1758836.
[23] Abdenour Abdelli., (2007) "Optimisation multicritère d'une chaîne éolienne passive ". PHD thesis of the national polytechnic institute of Toulouse., Plasma and Energy Conversion laboratory, order N°: 2519.